AD-A090 361 ARMY ELECTRONICS TECHNOLOGY AND DEVICES LAB FORT MON--ETC F/G 9/1
COMBAT HARDENED COMMUNICATIONS: HIGH PRECISION FREQUENCY CONTRO--ETC(U)
JUN 80 A BALLATO, T LUKASZEK

UNCLASSIFIED

NL

1 OF 1
AD A090361

END
DATE FILMED
11-80
DTIC

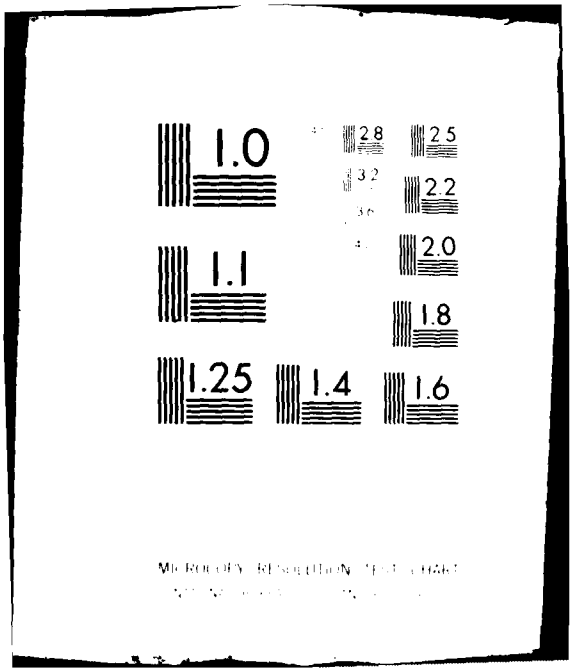
1.0
2.8
2.5
3.2
2.2
3.6
2.0
1.1
1.8
1.25
1.4
1.6

*BALLATO & LUKASZEK

COMBAT HARDENED COMMUNICATIONS: HIGH PRECISION FREQUENCY CONTROL USING RESONATORS IMMUNE TO ACCELERATION AND STRESS FIELDS

ARTHUR BALLATO, PhD
THEODORE LUKASZEK, Mr.
USA Electronics Technology & Devices Laboratory, ERADCOM
Fort Monmouth, NJ 07703

INTRODUCTION

Exceedingly stringent frequency control requirements follow from the performance specifications of the latest generations of command, control, communications, & intelligence (C^3I) systems, and systems for navigation and position location. Unfortunately, the crystal resonators, which are the stabilizing elements in the reference oscillators required in such systems, are frequency sensitive to acceleration fields produced by the dynamic environments surrounding land- and air- mobile use. These resonators are also susceptible to frequency shifts due to transient temperature variations and static stresses transmitted by their electrode and mounting systems. The acceleration effects lead to degradation of the short-term frequency stability, while the stress component contributes primarily to long-term aging and to distortions of the frequency-temperature behavior of the oscillator.

This paper describes quartz resonators that provide simultaneous compensation against both dynamic and static conditions, and that are compensated, moreover, against rapid temperature transients encountered in fast-warmup oscillators for manpack use.

The acceleration problem is minimized by utilizing a novel monolithic compound vibrator having a racemic structure to nullify the frequency shifts. Static compensation is achieved by means of unique lateral mounting contours, located so that nonlinear elastic constants cancel. Compensation of thermal transients comes about by use of a special, doubly rotated orientation of cut. We show that all

three features may be realized at one time to yield a highly stable quartz resonator immune to accelerations in any direction, and to boundary stresses and thermal transients. No additional electronics are required, nor are increases in size, weight, and power requirements necessary.

The resulting units are applicable to a wide variety of high precision frequency control uses, such as oscillators in shock/vibration environments (tanks, helicopters), sensors, position location (GPS), and collision avoidance systems. An examination of these various systems uses, or derivations of the frequency control requirements from performance specifications in any detail are not permitted due to space limitations.

The stringency of the frequency control requirements imposed by time-ordered secure operation in combat environments is such that they could not be met by conventional crystal resonators. The effects of vibration alone on conventional resonators would degrade their performance to the point where the unthinkable would be necessary: tanks and helicopters would have to turn off their motors in order to communicate!

Fortunately, recent breakthroughs, mentioned briefly above, are available to permit the requirements to be met. These developments are consistent with the chronology of progress in timekeeping accuracy shown in Figure 1 (1). The entry marked "quartz crystal" is representative of a laboratory standard of conventional design, using an AT cut crystal, and protected to the greatest possible extent from environmental disturbances. Its fractional frequency stability is about 5 parts in 10^9. Contrast this with a requirement of the Global Positioning System (GPS) calling for 100 meter range accuracy. To hold this accuracy for one day requires a stability of $100m/(3*10^8\ m/s * 86{,}400s) \simeq 4x10^{-12}$, or about a factor of one thousand better than the conventional laboratory standard of some years ago.

A parallel to GPS, as well as a contrast, is furnished by another entry on Figure 1: the marine chronometer built by John Harrison in 1759 (2). Its purpose was to determine longitude at sea by accurately keeping London time for comparison with local time determined on board ship from measurements of the sun or stars. Pendula-controlled escapements (Huygens, 1660) had proved useless at sea except in a dead calm. Harrison improvised new techniques to reduce the influences of ship motion and other environmental effects, and won the £20,000 prize offered in 1714 for a device that would determine the longitude within 30 minutes of arc (~56 km). The 56 km of

(180)

Harrison's time has shrunk to 100 meters in the GPS program (10 meters in the secure mode), but the environmental factors that must be overcome now are much the same as those he had to contend with: primarily temperature and motional effects.

We have mentioned GPS because of the obvious and interesting comparison with work more than two centuries old; it must be emphasized, however, that the environmental hardening features to be addressed below apply with equal cogency to other systems such as JTIDS, NIS, SINCGARS, SEEK TALK, etc.

In Figure 2 is shown an idealized frequency-time plot of a conventional quartz oscillator subjected to distrubances of various kinds. At time t_1 an abrupt temperature change produces a sharp frequency transient, followed by an asymptotic approach to a new frequency characteristic of the new temperature. A similar effect occurs between t_5 and t_6 where power shut-off followed by oscillator restart leads to mis-frequency operation that is of concern for fast-warmup manpack use. Between t_2 and t_3, at t_4 and again at t_7, are shown the effects of vibration, shock, and tip-over (reversal of crystal attitude with respect to the gravity field), respectively. These three effects are due to acceleration forces, and are not further distinguished in the sequel. Superimposed upon the collection of disturbances seen in Figure 2 is the long-term aging slope. The principal contributors to this are the slow change in electrode stress due to relaxation of the metal films deposited on the resonator plate surfaces and the relaxation of the mounting and support system; these will be discussed further below, as will be the fine-structure of the frequency-time curve labeled "short-term instability".

STATIC AND DYNAMIC TEMPERATURE EFFECTS

The standard frequency control element commonly used is the AT cut quartz resonator, a singly rotated plate, shown in Figure 3, with $\theta \sim +35^\circ$. Its traditional popularity is due to ease of manufacture coupled with a zero temperature coefficient (ZTC) of frequency at room temperature. A family of doubly rotated cuts of quartz possesses a ZTC; these are more difficult to manufacture because of the second angle ϕ. The locus of ZTC as function of θ and ϕ is shown for quasi-static temperature changes in Figure 3 (3). The cut marked "SC" on the locus at $\phi \sim 22^\circ$, $\theta \sim +34^\circ$ denotes the newly developed "stress compensated" resonator (4,5,6). Because the double rotation leads to manufacturing problems, growth of cultured quartz bars incorporating the first (ϕ) rotation has been undertaken (7) with the resulting bar shown schematically in Figure 4; SC cuts may be produced from these bars with a single cutting operation.

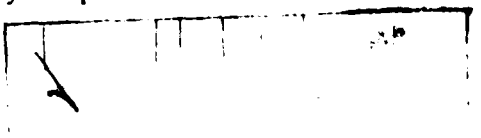

Figure 5 gives the frequency versus temperature (f-T) behavior for cuts located near the SC value when the temperature change is made very slowly. The inflection temperature is 96°C, and for small temperature departures about this value the frequency changes expected are small. The conventional AT cut has a similar cubic f-T shape, but with inflection temperature of 26°C. Operation of an AT cut in an oven with millikelvin stability leads to the conclusion, based on the static f-T curve, that frequency stabilities in the 10^{-15} range are possible, where, in fact, the observed stabilities are orders of magnitude worse. Figure 6 gives an example, showing the elliptical orbits that result from sinusoidal temperature variations having periods of 8 & 16 hours, and 1 week, superimposed on the static f-T curve (8). For the SC cut, this dynamic thermal stress effect is absent; it arises from nonlinear elastic constants which cancel at the SC orientation. The implications for fast-warmup operation are demonstrated in Figure 7 where AT and SC responses to oven warmup are shown. Note the logarithmic ordinate scale. The SC is on frequency in a time dictated solely by the oven; the AT transient effect persists much longer. Use of doubly rotated SC cuts effectively eliminates the transients that occur at times t_1 and t_5-t_6 in Figure 2.

STATIC FORCE EFFECTS

Static and quasi-static edge forces occur due to relaxation of the mounting and support structure holding the resonator and because of differential thermal expansion coefficients between the quartz and mount. These forces produce frequency shifts and distort the shape of the f-T curves of Figure 5. For diametric force pairs, shown on the right-hand illustration in Figure 8, the effect is quantified by a coefficient K_f that is directly proportional to the observed frequency shift $\Delta f/f$ and inversely proportional to the applied force F (9,10). K_f is a function of the plate azimuth ψ. Altitude contours of $K_f(\psi)$ are plotted in Figure 9 for doubly rotated plates having orientations along the upper ZTC locus in Figure 3. It is seen that for each cut (value of ϕ), azimuths (ψ) exist such that $K_f(\psi)$ becomes zero. At these angles of ψ edge forces do not produce frequency shifts. Mounting resonator plates at these points, however, produces large edge stresses with consequent susceptibility to breakage, especially in high shock applications such as REMBASS.

We have shown experimentally (11) that collinear forces acting upon chords trimmed from the circular resonator plate normal to the K_f=0 locations also produce no frequency shift. The case for the AT cut is seen in Figure 10. Forces acting at paired locations (1).. ..(6), for example, do not produce deviations in vibrator resonance

(192)

frequency. Superposition has also been shown to hold for multiple force-pairs, with the result that the entire chordal edge may be used for mounting, and the stress levels appreciably reduced without affecting frequency stability. As shown in Figure 11, which is again for the AT cut, the remaining circular boundaries may be trimmed to produce a rhomboid shape. The K_f=0 angles of ψ vary with the cut of quartz used, as shown in Figure 9; the rhomboidal outline required will also change. The outline for the ϕ=10° cut is given in Figure 12. Also shown on this figure are the four mounting edges, the "key-hole" electrode pattern normally used, and the offset of the electrode tabs from the crystallographic axis for the purpose of reducing undesired resonance modes. The asymmetrical rhomboid shape is characteristic of doubly rotated cuts; the AT cut of Figure 11 is symmetrical because X_1 is a two-fold axis of symmetry in quartz. For the SC cut (ϕ=21.9°), the rhomboid shape, by fortunate coincidence, degenerates to a square (or rectangular) outline, as shown in Figure 13. All four edges are used for mounting, which may be extremely rigid. The plate itself must be cut with respect to the crystallographic axes at an angle of 36.8° as shown, in order to possess the static force insensitivity property. SC cuts with square outline are self-aligning when placed in ceramic flatpack holders, a feature that leads to reduced cost of manufacture.

DYNAMIC FORCE EFFECTS

The dynamic force effects illustrated in Figure 2 at times t_2-t_3, t_4 and t_7 are subsumed under the phrase "acceleration effects". They may range from the shocks of cannon launching (20,000 g's) to vibrations due to microseisms of a few micro-g's. The typical level of sensitivity of AT cut resonators is 10^{-9} per g - seemingly a small number for many applications (the average shock level for trucks is a few g's), until contrasted with the typical value given in the introduction for GPS, or indeed with the accuracies that are quoted for any of the modern C^3I systems.

Experimental data provided by Valdois (12) for AT cut quartz is shown in Figure 14. It is seen that the frequency shift depends upon the direction of the acceleration field, and, more importantly, is a linear function of the acceleration G, changing sign with reversal of G. This observation is the key to producing acceleration-immune resonators, for if two resonators can be paired so that their respective crystallographic axes are antiparallel, then the frequency shifts induced by an acceleration field in any arbitrary direction will be opposite in the two resonators and thus cancel in the combination (13). The required antiparallelism can be produced by using

(183

enantiomorphous pairs of resonators (right- and left-handed crystals), a feature that very fortunately exists in quartz. In Figure 15 are shown stacked crystal plate resonator combinations configured for parallel (left drawing) and series electrical connection. Each stack consists of a left-handed and a right-handed, singly rotated (e.g. AT) cut, identical except for the handedness, bonded together to form a composite resonator requiring no increase in size, weight and power for its operation over a single resonator of thickness equal to twice that of either racemic half of the stack. The plates are drawn with rectangular outline for clarity; in practice they would be of rhomboid contour as discussed above.

Modeling of the physics of these structures is best accomplished by means of equivalent electrical networks. These have never taken into account the handedness of the crystal, so we have developed the network of Figure 16 to accomplish this. The transmission line represents the acoustic waves in the thickness mode plate; the mechanical ports CD and EF account for the mechanical boundary conditions (traction free surface = short circuit); the electrical port AB is connected to the oscillator; the mechanism of piezoelectric transduction is represented by the transformers located at the plate surfaces to produce tractions. Placement of the transformer polarity dots characterizes the crystal handedness for the purposes required for simulations. The effect of acceleration is simply incorporated into the transmission line parameters. Using two networks of different handedness, the structures of Figure 15 may be accurately modeled.

Doubly rotated (e.g. SC cut) plates represent an additional degree of difficulty when considering stacked resonators - or seemingly so. These resonators exhibit the same type of behavior as seen in Figure 14, but whereas the symmetry of AT-cut quartz leads to simple vibratory motion (thickness-shear with motion along the X axis), doubly rotated plates such as the SC cut have particle motion inclined to the crystal axes. It at first appears that stacking two plates would produce mode interference, but this is not so. In Figure 17 is shown on the left a left-handed plate with motion taken to be along the major diagonal OA; the center illustration is the situation that obtains with the mirror-image right-hand mate. The right-handed plate has motion along OB. When the right-handed plate is properly rotated as shown in the right-most illustration, the particle motion during vibration is seen to be parallel to that of OA in the left-most illustration, so that stacking can take place with respective crystallographic axes antiparallel, as is necessary for acceleration compensation.

(194

It should be emphasized that the compensation holds for any direction of the acceleration field, and no preferred orientation of the composite stack is necessary.

Networks for left- and right-handed plates are shown joined in Figure 18 to represent a composite resonator. The electrical terminals are connected either in parallel or series to achieve the structures of Figure 15. Inductors represent electrode mass loading on the crystal surfaces, and the 1:-1 mechanical transformer models the reversal of crystal axes to form the acceleration-immune stack.

COMPENSATION FOR ADDITIONAL EFFECTS

It was mentioned earlier that the long-term aging slope seen in Figure 2 arose largely from electrode stress relief. In Figure 19 is shown the graphs of the static force coefficient $K_f(\psi)$ verses ψ for the three thickness modes in the SC cut. For the "c mode" (the slower shear mode having the thermal transient compensation property described above), it may be shown (14) that the area under the curve of $K_f(\psi)$ vs ψ is zero. Because superposition holds for point force-pairs, one may show the direct proportionality between the film stress coefficient K as portrayed on the left of Figure 8, and calculated in Figure 20, and the angle-average coefficient $\langle K_f \rangle$; this relation is also given in Figure 20. Calculating $\langle K_f \rangle$ for the cuts on the upper ZTC locus of Figure 3 and comparing with experiment gives the results of Figure 21, where it is seen that the film stress effect produces no frequency change, and consequent aging, for the SC cut.

Cancellation of the nonlinear elastic constants responsible for thermal and mechanical effects in quartz resonators at the SC orientation is additionally responsible for lessening the phase noise contribution to the short-term instability seen in Figure 2.

CONCLUSION

We have made available quartz resonator configurations frequency compensated for acceleration, static forces, thermal transients and other effects encountered in combat, and more benign environments. These units are comprised of:

- doubly rotated, SC-cut orientations
- rhomboidal contours for mounting
- stacked enantiomorphous pairs

combined in a rugged unit of exceptional stability requiring no increases in size, weight or power consumption. Anticipated oscillator

195

stabilities with these resonators for the 1985-1990 time-frame are:

stability	1 sec	10^{-14}
	24 hours	10^{-13}
	5 years	10^{-10}

acceleration sensitivity < 10^{-12}/g.

REFERENCES

1. J.A. Barnes, "Basic Concepts of Precise Time and Frequency", in Time and Frequency: Theory and Fundamentals, (B.E. Blair, ed.), NBS Monograph 140, May 1974. U.S. Government Printing Office, Washington, DC 20402, pp. 1-40.

2. L.A. Brown, "The Longitude", in The World of Mathematics, (J.R. Newman, ed.). Simon and Schuster, New York, 1956. Volume 2, pp. 780-819.

3. R. Bechmann, A. Ballato, and T.J. Lukaszek, "Higher-Order Temperature Coefficients of the Elastic Stiffnesses and Compliances of Alpha-Quartz", Proc. IRE, Vol. 50, August 1962, pp. 1812-1822.

4. E.P. EerNisse, "Calculations on the Stress Compensated (SC-cut) Quartz Resonator", Proc. 30th Annual Frequency Control Symposium, US Army Electronics Command, Fort Monmouth, NJ 07703, June 1976, pp. 8-11.

5. J.A. Kusters, "Transient Thermal Compensation for Quartz Resonators", IEEE Trans. Sonics Ultrason., Vol. SU-23, July 1976, pp. 273-276.

6. A. Ballato, "Doubly Rotated Thickness Mode Plate Vibrators", in Physical Acoustics:Principles and Methods (W.P. Mason and R.N. Thurston, eds.) Vol. 13, Chap. 5. Academic Press, New York. 1977, pp. 115-181.

7. Sawyer Research Products Inc., Eastlake, OH 44094; Motorola Inc., Carlisle, PA 17013.

8. A. Ballato, "Static and Dynamic Behavior of Quartz Resonators", IEEE Trans. Sonics Ultrason., Vol. SU-26, July 1979, pp. 299-306.

9. A. Ballato, "Force-Frequency Compensation Applied to Four-Point Mounting of AT-Cut Resonators", IEEE Trans. Sonics Ultrason., Vol. SU-25, July 1978, pp. 223-226.

(196)

10. E.P. EerNisse, T. Lukaszek, and A. Ballato, "Variational Calculation of Force-Frequency Constants of Doubly Rotated Quartz Resonators", IEEE Trans. Sonics Ultrason., Vol. SU-25, May 1978, pp. 132-138.

11. T.J. Lukaszek and A. Ballato, "Resonators for Severe Environments", Proc. 33rd Annual Frequency Control Symposium, US Army Electronics Command, Fort Monmouth, NJ 07703, May-June 1979, pp. 311-321.

12. M. Valdois, "Étude de l'Influence d'Accélérations sur les Propriétés des Resonateurs à Quartz", Thèse, Université de Besançon, June 1974, 73 pp.

13. A. Ballato, "Resonators Compensated for Acceleration Fields", Proc. 33rd Annual Frequency Control Symposium, US Army Electronics Command, Fort Monmouth, NJ 07703, May-June 1979, pp. 322-336.

14. A. Ballato, E.P. EerNisse, and T.J. Lukaszek, "Experimental Verification of Stress Compensation in the SC Cut", Proc. IEEE Ultrason. Symposium, September 1978, pp. 144-147.

(197)

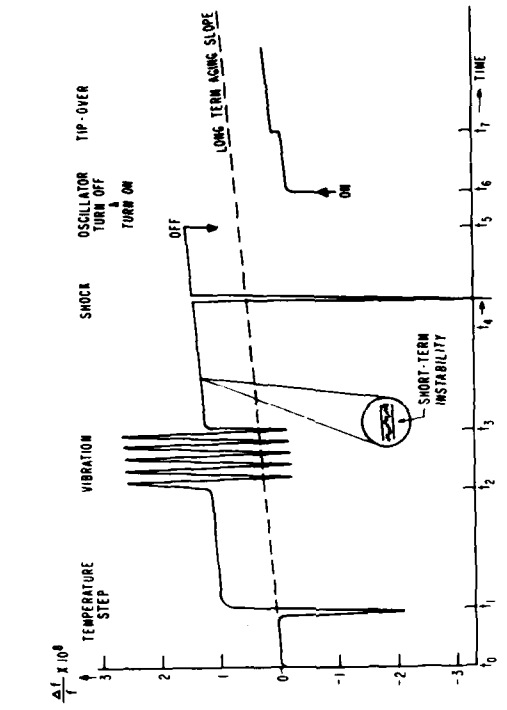

Fig. 2 - Idealized Frequency-Time Behavior of a Quartz Oscillator

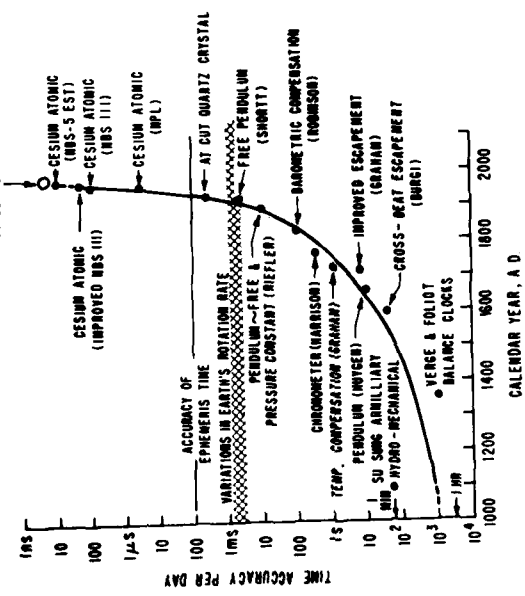

Fig. 1 - Progress in Timekeeping Accuracy

(188)

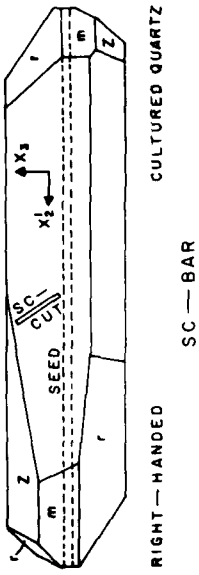

Fig. 4 - Quartz Bar Showing SC Cut

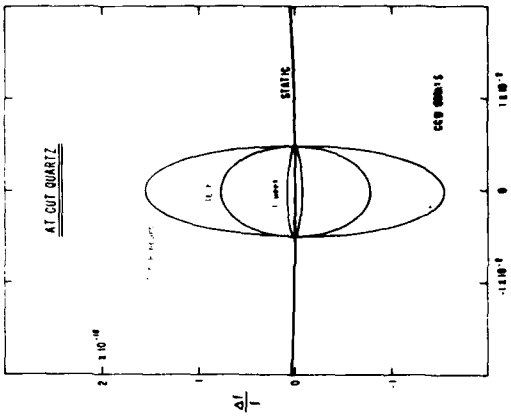

Fig. 6 - Dynamic Frequency-Temperature Behavior

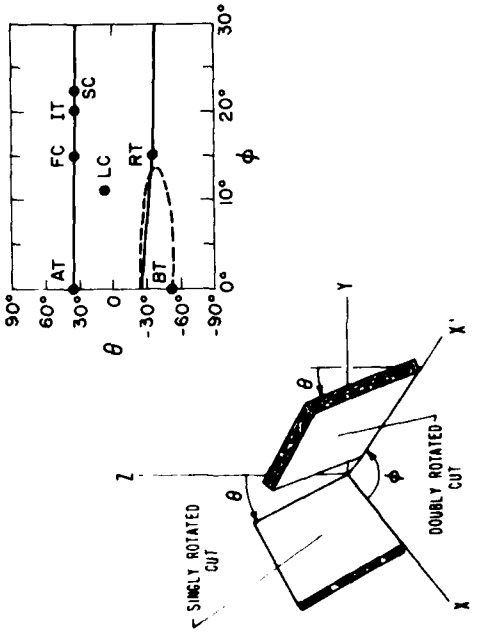

Fig. 3 - Rotated Quartz Cuts and Temperature Coefficients

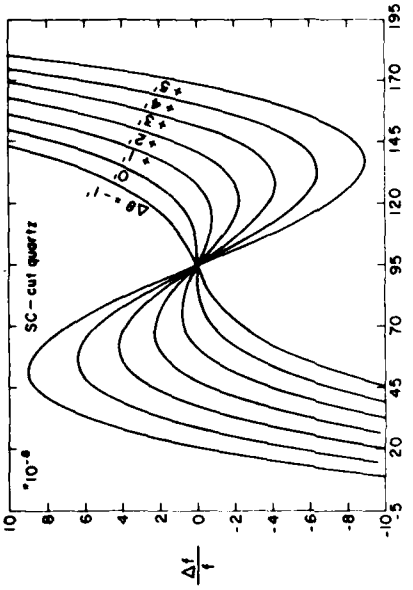

Fig. 5 - Static Frequency-Temperature-Angle Plots

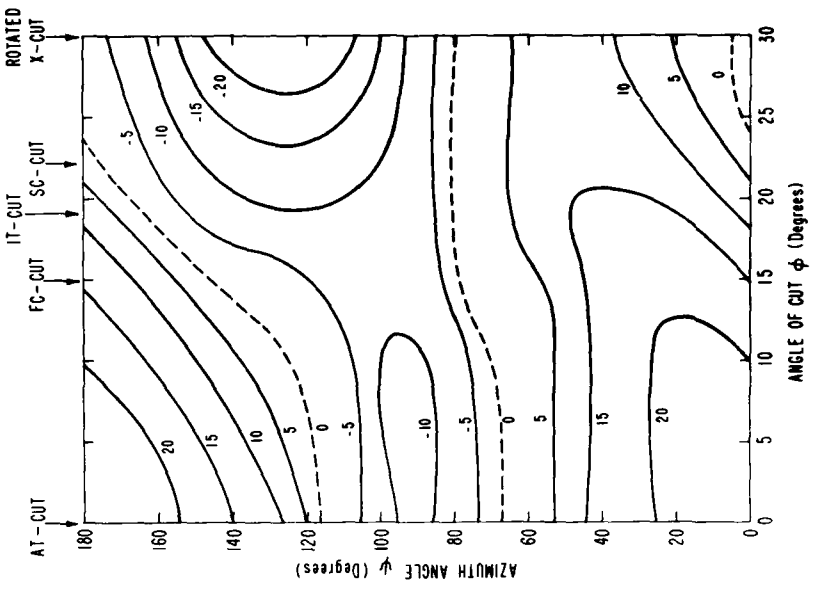

Fig. 9 - Contours of Force Coefficient K_f : Mode a (10^{-15} m . s / N)

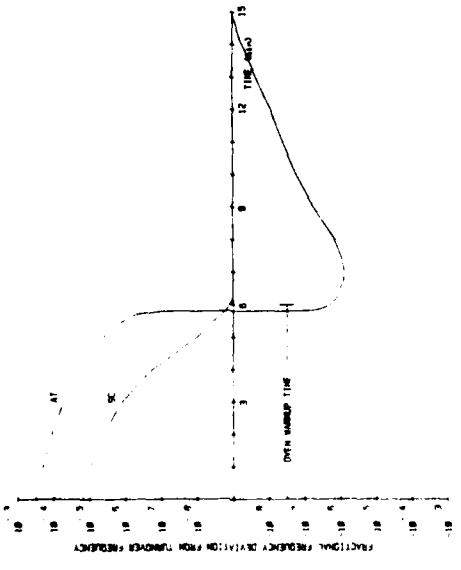

Fig. 7 - Warmup Characteristics of AT and SC Resonators

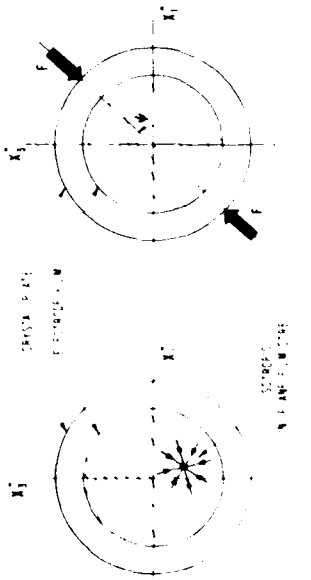

Fig. 8 - Schematics of In-Plane Film Stress and Static Edge Force

190

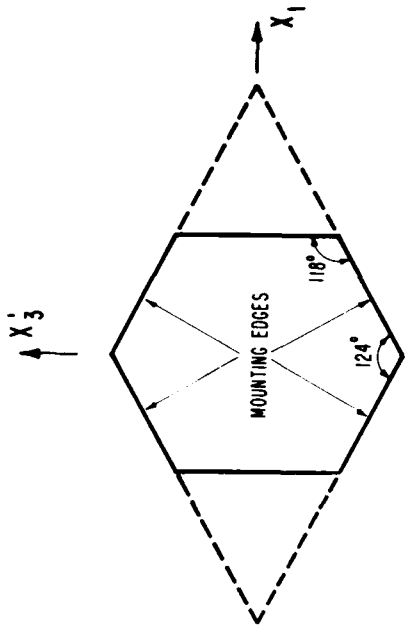

Fig. 11 - AT Cut Polygon for Minimum Force-Frequency Effect

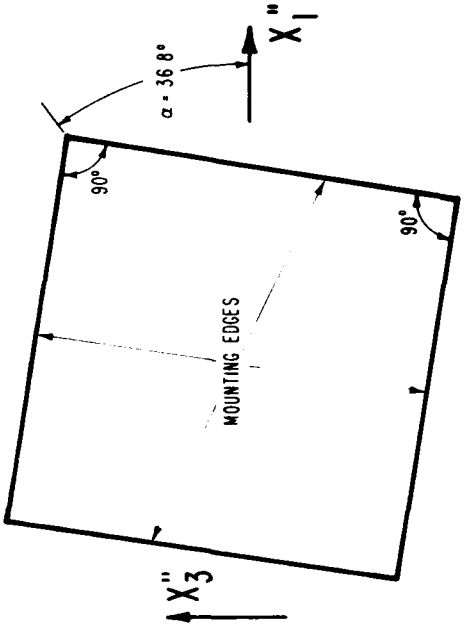

Fig. 13 - SC Cut Polygon for Minimum Force-Frequency Effect

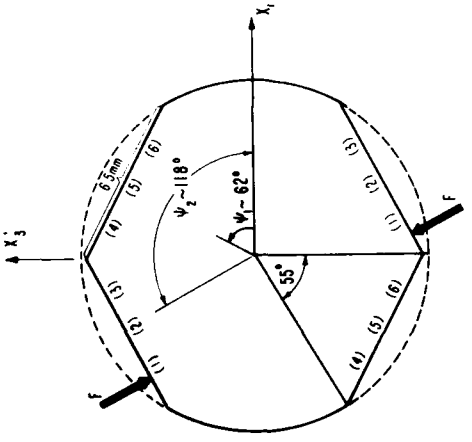

Fig. 10 - Rhomboid Configuration Construction

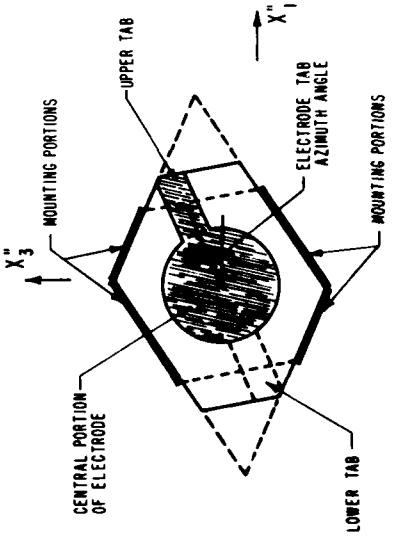

Fig. 12 - Polygonal Resonator with Electrode/Mounting Tabs

(191)

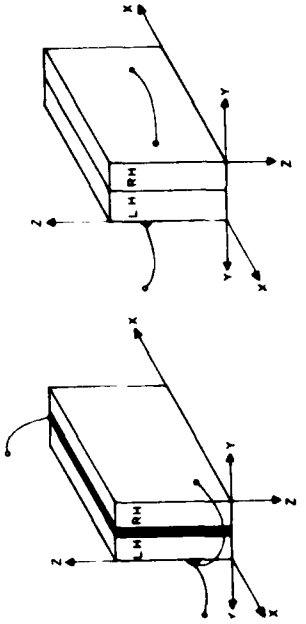

Fig. 15 - Stacked-Crystal Enantiomorphs for Parallel and Series Connections

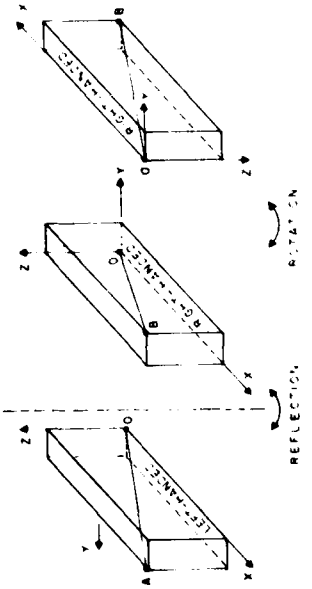

Fig. 17 - Doubly Rotated Enantiomorphs for Stacking

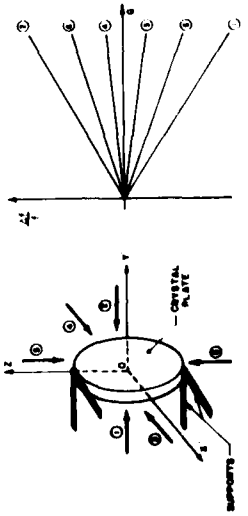

Fig. 14 - Experimental Acceleration-Frequency Behavior

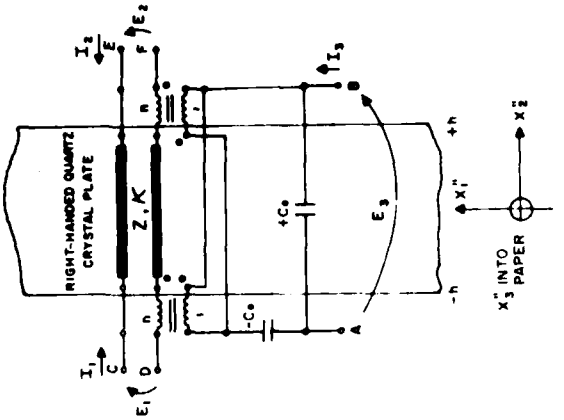

Fig. 16 - Single Resonator Transmission Line Network

(192)

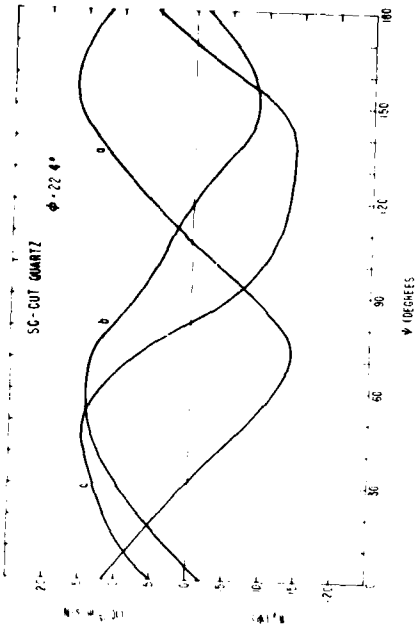

Fig. 19 - SC Cut Force Coefficients: a, b, & c Modes

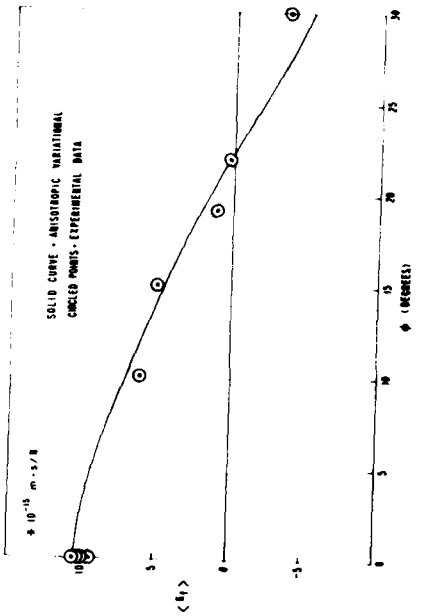

Fig. 21 - Average Edge Force Coefficients vs Angle of Cut

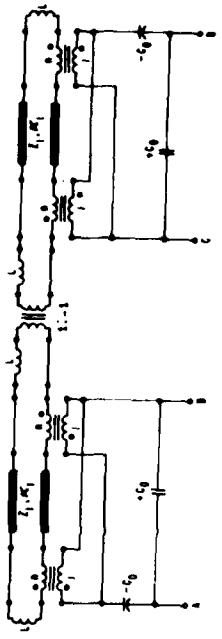

Fig. 18 - Stacked-Crystal Transmission Line Equivalent Network

FILM STRESS:

$$\frac{\Delta F}{F} \Big/ \frac{\Delta f}{f_0}$$

$$\frac{2}{\pi}, \quad (F/2H \cdot \rho)$$

EDGE FORCE:

$$k_F(\psi) = \frac{(2H \cdot E/F)}{\lambda_0}, \quad \frac{\Delta F(\psi)}{F}$$

$$\langle \gamma_F \rangle = \frac{1}{\pi} \int_0^{\pi} k_F(\psi)\, d\psi$$

$$\langle \gamma_F \rangle = \frac{2}{\pi} \cdot \frac{F}{\lambda_0}$$

Fig. 20 - Relation between Film Stress and Average Edge Force Coefficients

(193) -194x